

Tensile behaviour of mortar-based composites for externally bonded reinforcement systems

Stefano, De Santis^a and Gianmarco, de Felice^{b,*}

^a Department of Engineering, Roma Tre University, Via Vito Volterra 62, 00146, Rome, Italy.

E: stefano.desantis@uniroma3.it. T: +39 06 5733 6387. F: +39 06 5733 3441.

^b Department of Engineering, Roma Tre University, Via Vito Volterra 62, 00146, Rome, Italy.

E: gianmarco.defelice@uniroma3.it. T: +39 06 5733 6268. F: +39 06 5733 3441. *Corresponding author.

ABSTRACT

Textile reinforcements applied with inorganic matrices are currently receiving great attention for strengthening reinforced concrete and masonry structures, especially when preservation criteria need to be fulfilled for safeguarding cultural heritage. As the development of mortar-based reinforcements is still at an early stage, their mechanical properties need to be investigated and standardized testing methodologies have to be defined. The paper presents an experimental study on the tensile behaviour of strengthening systems comprising two different textiles and five mortar matrices. Various clamping methods and testing setups have been experimented and their effect on the results is discussed. Monotonic and cyclic tests have been carried out to derive strength and stiffness, crack pattern, failure mode, and response stages under tension, which have been related to the mechanical properties and the layout of the matrix and the textile.

KEYWORDS

B. Mechanical properties, B. Strength, D. Mechanical testing, Mortar-based composites

1. INTRODUCTION

Externally bonded reinforcement (EBR) systems with composite materials are becoming a widely used technique for repairing and strengthening existing structures, since they provide significant strength improvement without altering geometry, mass and stiffness of the structural members. The use of epoxy resin-based composites, such as Fibre Reinforced Polymers (FRPs), is currently discouraged for applications to masonry structures since the presence of epoxy matrix may prevent a proper transpiration of the substrate thus compromising preservation and durability. Innovative strengthening systems based on textiles embedded into inorganic matrices have been recently proposed [1,2], which, compared to FRPs, ensure better performances at high temperatures, better material compatibility and vapour permeability, lower cost and time of installation on uneven surfaces, and are

1 therefore suitable especially for use on masonry substrates. Furthermore, mortar-based reinforcements appear
2 particularly promising for application to cultural heritage, for which additional specific requirements must be
3 satisfied: (i) respect of authenticity in terms of materials and structural behaviour, (ii) principle of minimum
4 intervention, (iii) reversibility, intended as substitutability and removability, (iv) compatibility with original
5 substrates and decorative settings, (v) durability [3].
6

7
8 Differently from FRPs, for which a consolidated knowledge has already been gained (see, amongst others: [4,5]),
9 the study of mortar-based EBRs is still at an early stage. A limited number of laboratory studies have been
10 carried out to date, devoted to material behaviour and composite-to-substrate bond performance [6-11] as well as
11 to rehabilitation solutions for both masonry [12-13] and reinforced concrete [14-15] structures. Despite some real
12 applications already exist [3,16-17], a deeper knowledge needs to be developed before mortar-based systems can
13 be confidently used for safeguarding existing structures, especially when belonging to the built heritage.
14

15
16 There are some structural applications (such as the extrados strengthening of arches and vaults with mechanical
17 end anchors/pivots, the confinement of masonry columns and of reinforced concrete pillars and nodes) in which
18 the tensile behaviour of EBRs plays a particularly important role and maximum attainable stress can be fully
19 exploited. Differently, for a broad range of applications (e.g., the strengthening reinforcement of masonry panels
20 towards both in-plane and out-of-plane loads, the bending reinforcement of masonry jack arches and of r.c.
21 beams), failure is generally due to debonding. In these cases, tensile tests provide fundamental design parameters
22 such as the tensile modulus of elasticity of the composite, the matrix-to-textile bond properties, which may
23 significantly affect cracking, adhesion to the substrate, and durability. For these reasons, direct tensile tests are
24 required by standard codes [18-19] for the mechanical characterization of mortar-based reinforcements and are
25 expected to become a fundamental step of the industrial process for product qualification purposes. Nevertheless,
26 an improved knowledge still needs to be gained on the tensile response of mortar-based composites, and
27 standardized testing methodologies, specifically conceived for this type of strengthening systems, have not been
28 defined yet. Numerous features need to be specified, including testing setup and equipment, gripping methods,
29 fundamental outcome parameters, expected results. Scientific technical committees (such as RILEM TC 250-
30 CSM - Composites for Sustainable Strengthening of Masonry) and standardization commissions at national and
31 European level have been lately activated with this aim.
32

33
34 Recent research on Textile Reinforced Concrete (TRC) [20] can provide useful information thanks to the
35 analogies with mortar-based EBR systems. Numerous experimental studies have been carried out in the last
36 decade on the tensile response of TRC [21-22], also including effects of testing procedures and setup detailing
37
38
39
40
41
42
43
44
45
46
47
48
49
50
51
52
53
54
55
56
57
58
59
60
61
62
63
64
65

[23-24]. However, TRC matrices usually consist of high performance cement concrete, which may be suitable for the strengthening of reinforced concrete members, while application to masonry usually involves weaker lime mortars. As for the fibres, beyond glass, carbon and aramid textiles, which are generally used in TRC, steel cords [16], basalt [25] and natural fabrics [26] have been proposed for the reinforcement of masonry. Such a large variability of textiles and matrices may result in a particularly wide range of possible responses in terms of crack development, failure mode, and ultimate state behaviour.

This paper presents an experimental study on eight mortar-based strengthening systems under tensile loading. Specimens have been manufactured using two fabric types, such as glass-aramid and steel. The former is made out of bidirectional bundles of wires, and is already widely used for manufacturing TRC and polymer based composites. The latter consists of unidirectional high strength steel cords, and is less common than other fibrous textiles (e.g., carbon, glass, and basalt) even if steel is a traditional construction material. Five matrices have been used, ranging from strong pozzolan mortar to relatively weak hydraulic lime mortar. As a first step, different clamping methods have been experimented to identify an appropriate testing setup, according to the properties of the specimen under investigation. Then, tensile tests have been carried out to derive stress-strain relationships and the mechanical behaviour at the different response stages, from the un-cracked stage, to the crack development, up to failure. A full characterization of the strengthening systems is derived, aiming at contributing to the existing knowledge for the reinforcement design under Ultimate Limit State conditions. Finally, cyclic tests have been performed to derive residual crack width and hysteretic response, related to Damage Limit State conditions and durability requirements.

2. MATERIAL PROPERTIES AND TESTING SETUP

2.1. Properties of textiles and mortars

Two textiles have been used, whose mechanical properties have been derived by tensile tests, as reported in Section 3.1.:

- an unbalanced bidirectional fabric (G) made out of glass and aramid yarns in warp direction and of glass yarns in weft direction, coated to improve matrix-to-textile bond and durability (Fig. 1a);
- a unidirectional mesh of galvanized Ultra High Tensile Strength Steel (UHTSS) cords, with two different densities, 4 cords/inch (S4) (spacing 6.35mm, Fig. 1b) and 12 cords/inch (S12) (spacing 2.12mm, Fig. 1c).

1 The following matrices have been used: a mineral mortar (M) with a binder of natural kaolin and bauxite fired at
2 1000-1200°C; a cement mortar (C) with pozzolan and polypropylene microfibres; a polymer modified cement
3 mortar (P) comprising 1% cellulose microfibres to hold water during hardening and prevent shrinkage; a mineral
4 mortar (ML) with natural kaolin, bauxite and hydraulic lime binders; and, finally, a natural hydraulic lime (L)
5 mortar. Eight types of composite specimens have been manufactured, as listed in Table 1, in which the average
6 properties of the matrices are also specified: compressive strength (f_{mc}) (derived from tests on cubic specimens)
7 and Young's modulus (E_{mc}) (from compression tests on cylinders), tensile strength (f_{mt}) (from three point
8 bending tests), and grain size range (D). Due to chemical composition and mechanical properties, mineral,
9 polymer-modified and cement mortars are mainly suitable for reinforced concrete members, and contemporary
10 masonry types and infill panels, while lime mortars might be preferred for historic substrates, especially when
11 interactions with decorative settings (e.g., frescos and paintings, plasters, valuable stones, etc.) are expected.
12
13
14
15
16
17
18
19
20
21
22
23

24 **2.2. Testing setup**

25
26 Tensile tests have been carried out using a Material Testing Systems (MTS) load frame (Fig. 2). Load was
27 applied by a 500kN hydraulic actuator under displacement control at 0.01mm/s rate (machine compliance
28 <0.05%), and recorded by a load cell with 0.2% accuracy and 0.01kN resolution. Three different devices have
29 been used to record strains/displacements. Global measures were acquired by a Linear Variable Differential
30 Transformer (LVDT) and, only for composite specimens, two linear potentiometers (Fig. 2b). The former was
31 integrated in the testing machine and recorded the relative displacement from end plate to end plate with 0.05%
32 accuracy and <1µm resolution. The potentiometers were fixed on the mortar by means of aluminium plates (Fig.
33 2b) with a base length of about 250mm, and had ±12.5mm range, 0.15% accuracy, and <10⁻⁴mm resolution. The
34 redundancy of two global measures allowed for the detection of possible sliding of the specimen in the gripping
35 areas. Finally, a MTS extensometer having 50mm gage length, +25/-5mm range, 0.18% accuracy and <10⁻⁵
36 resolution, was placed in the middle of both textile and composite specimen (Figs. 2a,b) to accurately record
37 local strains and confirm the reliability of global measures. Clearly, in composite specimens the extensometer
38 provides reliable strains only before cracking, especially when the crack spacing is larger than its measurement
39 base, as it will be shown afterwards. Test data were acquired at 10Hz frequency by means of a National
40 Instruments NI PCI 6281 Multifunction Data Acquisition (DAQ) system, provided with 3 units NI SCXI 1520
41 Universal Strain-Gauge Input Module, with 8 Channels each; the acquisition software was developed in
42 LabView environment.
43
44
45
46
47
48
49
50
51
52
53
54
55
56
57
58
59
60
61
62
63
64
65

2.3. Clamping methods

As the clamping method may significantly influence the measured strength [24], five different procedures have been experimented to identify suitable techniques that avoid local stress concentrations in the vicinity of the clamping wedges, and ensure at the same time minimum effort in specimen preparation and installation [23].

Fig. 3 illustrates the clamping methods, while Fig. 4 shows the stress-strain curves of specimens manufactured with glass-aramid mesh and mineral mortar (G-M series), gripped with the experimented methods, in order to emphasize the effect of clamping on the response.

The easiest and quickest method consisted in leaving the ends of the specimen free of mortar and clamping the textile directly in the wedges (Clamping Method CM-A, Fig. 3a). By doing so, however, a premature rupture of the fibres occurred exactly at the edge of the grips, providing an underestimate of the ultimate load (Figs. 3b, 4). To prevent the textile from being cut by the grips, aluminium tabs (90mm×50mm×3mm) have been glued to the specimen ends (free of mortar) by means of a strong structural adhesive (CM-2, Fig. 3c). Aluminium was preferred to steel because of its higher deformability, allowing for a better stress transfer. A careful smoothing of the tabs and a sufficient amount of adhesive were necessary to ensure an adequate contact with the textile and prevent its premature rupture. This clamping method resulted however unsatisfactory as the specimen failed at the beginning of the mortar matrix (Fig. 3d), because of a localized variation of the axial stiffness. A slight underestimate of strength is also suggested by the comparison with other methods (Fig. 4).

In order to avoid premature failure in proximity of the matrix end, a FRP reinforcement (bidirectional carbon fabric glued with epoxy resin) was applied to each specimen end (CM-3, Fig. 3e). Then, aluminium tabs were glued; their internal surfaces were smoothed to avoid the rupture of the fibres. At the same time, an undesirable deflection of the reinforcement textile was carefully avoided during FRP application, as this could cause the systematic application of an out-of-plane parasitic bending moment. With this gripping method, no premature failure occurred and the full development of transverse cracks was observed during the tests. Rupture took place in an intermediate section (Fig. 3f). The comparison between the readings of the LVDT (recording the relative displacement between the clamping wedges) and of the potentiometers (applied to the mortar, Fig. 2b), made it possible to detect if the textile was slipping within the mortar in the vicinity of the gripping areas. The experimental tests indicated that some slippage of the glass-aramid yarns occurred at the beginning of the tests in the first segment of the textile embedded in the mortar matrix (where cracking was prevented by FRP reinforcement). As a consequence, a portion of the strain was not recorded by the potentiometers, leading to both an overestimate of the initial stiffness and an underestimate of the strain corresponding to the peak stress (Fig.

1
2
3
4
5
6
7
8
9
10
11
12
13
14
15
16
17
18
19
20
21
22
23
24
25
26
27
28
29
30
31
32
33
34
35
36
37
38
39
40
41
42
43
44
45
46
47
48
49
50
51
52
53
54
55
56
57
58
59
60
61
62
63
64
65

4). Conversely, no sliding was observed in steel-based composites, which offered a better cord-to-mortar interlocking. Therefore, clamping method CM-3 was used for running tests on these specimens.

The three gripping methods CM-1, CM-2 and CM-3 are particularly relevant to capture the behaviour of the reinforcement in those structural applications in which the load is applied to the textile, such as the confinement of columns, pillars, and nodes, and the extrados strengthening of arches and vaults with mechanical anchorages at both ends of the reinforcement strip. In other applications (such as the out-of-plane restraining and the in-plane strengthening of masonry walls, and the bending reinforcement of beams, panels, and jack arches), the load is instead transferred from the substrate to the matrix by means of shear bond stresses, and then to the textile through mortar-to-textile bond/interlocking. In order to represent this mechanism, two further gripping methods have been experimented, in which the load is applied to the mortar. Clamping method CM-4 (Fig. 3g) comprises a ringbolt gripped by the testing machine, a shackle and two holed aluminium tabs, glued to the mortar matrix, placed in series. While gluing the tabs, particular attention was paid in aligning their holes to the specimen axis, in order to avoid bending. The spherical articulation minimizes parasitic bending moments, as recommended by the Annex A of the US standard AC434 [19] and already tested for TRC specimens in [22-23]. With this clamping method, the textile slid within the matrix (Fig. 3h), especially with the glass-aramid fabric, due to the poor fabric-to-mortar interlocking. Generally, one single crack formed and enlarged, splitting the specimen in two halves, which progressively separated, giving rise to very large displacements/strains (Fig. 4), without reaching the textile rupture. Therefore, this clamping method appeared unsuitable to characterize the whole tensile behaviour up to failure of mortar-based composites.

Finally, the specimens were clamped directly on the mortar matrix after having applied an FRP reinforcement in the gripping areas, to prevent crushing (CM-5, Fig. 3i). This gripping method succeeded in ensuring an adequate load application to both textile and matrix, and in avoiding sliding in the gripping areas (Fig. 4), allowed for the development of transverse cracks during load application (Fig. 3j), and was therefore used for running tensile tests on glass-based systems. Nevertheless, it should be stated that this conclusion cannot be generalized to other textiles, since either a higher tensile strength, the lack of coating, or an insufficient interlocking may induce a premature pull-out of the textile [21].

3. TEST RESULTS

Monotonic tensile tests have been carried out on 6 specimens for each textile and composite type, for a total of 24 tests on dry textiles, and 48 monotonic tests on composite strengthening systems. In addition, 3 cyclic test have been carried out on two composite types. Tables 2 and 3 collect the mean values and the corresponding

Coefficients of Variation of the main outcome parameters for each series, while the response curves and the results of all the specimens are represented in the plots in Figs. 5, 8, 9, and 10.

3.1. Textile specimens

Aiming at characterizing the textiles under tension, 12 specimens of glass-aramid mesh (6 in warp direction and 6 in weft direction, in both cases comprising three bundles in the loading direction) and 12 specimens of steel cords (6 of S4 textile, comprising a total of 8 cords, and 6 of S12 textile, comprising 24 cords) have been tested, all having 600mm length. Aluminium tabs (90mm×50mm×3mm) were glued on their ends to ensure adequate clamping. Strains were derived locally by the extensometer and globally by dividing the LVDT displacement by the initial distance between the clamping wedges. Stresses were computed as the recorded load divided by the cross section area of the textile (defined as the product of width and design thickness) in the direction of loading. The design thickness, also named as equivalent or nominal thickness, is derived as the bulk density of the material divided by the surface density of the textile [18]. The resulting stress-strain response curves are shown in Figs. 5a and 5b for glass-aramid mesh and steel textiles, respectively. Apart from an apparent stiffness increase in the very first part of the curve, which is due to the progressive load transfer to the whole specimen, a linear elastic phase can be clearly detected. The tensile modulus of elasticity, computed between 30% and 60% of the peak stress, is, for the glass-aramid mesh, 101.5kN/mm² in warp direction (comprising aramid yarns) and 73.9kN/mm² in weft direction (entirely made out of glass fibres). For both S4 and S12 steel textiles, the tensile modulus of elasticity is 184kN/mm² (see Table 2).

A brittle failure occurred in glass-aramid mesh, characterized by the close progressive rupture of the glass yarns and, eventually, by that of the aramid yarns. The average peak stress (f_t) is 1829N/mm² in warp direction, and 1159N/mm² in weft direction, due to the absence of the (stronger) aramid bundles. Conversely, in steel textiles a loss of linearity occurs, followed by a nearly simultaneous rupture of the cords. The tensile strength is 3207N/mm² for 4 cords/inch textile (S4) and 3082N/mm² for 12 cords/inch textile (S12). Beyond the physiological scatter of experimental data, the slightly lower peak stress of S12 with respect to S4 may be due to the non-uniform load distribution among the cords, as a consequence of unavoidable (howsoever small) misalignments which may occur while clamping. All the experimental results (strength, peak strain and tensile modulus of elasticity) of the tests on textiles present very low scatter: the Coefficient of Variation is between 0.7% and 7.5%, as reported in round brackets in Table 2.

3.2. Composite specimens: monotonic tests

1
2 Prismatic composite specimens, having about 600mm total length and 50mm×10mm cross section, were casted
3
4 in Plexiglas frameworks according to European Standards [27-28] and cured for at least 28 days under laboratory
5
6 conditions (21±2°C and 60±5%RH). Six tests have been carried out on the eight composite types listed in Table
7
8 1. The results are represented in terms of mean-stress mean-strain relationships. Strains have been evaluated
9
10 either from the extensometer (before cracking), or from the LVDT and the potentiometers, dividing the recorded
11
12 displacements by the measurement base of the device, as discussed in Section 2.2. Stresses have been evaluated
13
14 as the applied load divided by the cross section area of the textile (as suggested by the codes [18-19] and done in
15
16 [24] for TRC, and in [2] for mortar-based reinforcements). By doing so, the possible variations of mortar cross
17
18 section (which are unavoidable, especially in field applications) do not affect test results. A characteristic stress-
19
20 strain response curve of a mortar-based reinforcement system under tension is shown in Fig. 6, while the crack
21
22 pattern evolution is depicted in Fig. 7. Three behaviour stages can be identified, such as un-cracked (I), crack
23
24 development (II) and crack widening (III), as already revealed by previous studies (see, amongst others: [2,29]).
25
26 As a general trend, in stage I the response is linear and the mortar provides a considerable contribution to both
27
28 load bearing capacity and stiffness. As soon as the stress exceeds the tensile strength of the matrix, cracks
29
30 develop and a reduction of stiffness is recognisable. First cracks generally form in the middle of the specimen
31
32 (Fig. 7a) and in the vicinity of its ends. Subsequent cracks occur between existing ones (Fig. 7b) until crack
33
34 number stabilizes. In the last stage (III) additional imposed strain results in widening of existing cracks, rather
35
36 than in developing of new ones, and mortar fragments are expulsed (Fig. 7c). Failure occurs as a result of the
37
38 tensile rupture of the reinforcement (Fig. 7d). Generally, one yarn/cord fails first and the progressive rupture of
39
40 the other ones follows.
41

42 The following design parameters have been derived from tensile tests on mortar-based strengthening systems:

- 43 • The ultimate stress (f_t), the corresponding strain (ϵ_t) and the tensile modulus of elasticity in the last stage
44
45 (E_{III}), which mainly depend on the properties of the reinforcement textile, and may be decisive for the
46
47 structural applications in which high stresses are applied directly to the fabric. The mean values of these
48
49 parameters are collected in Table 2 together with the corresponding CV. The ultimate load per unit
50
51 width (F_t) is reported as well to allow comparisons.
52
- 53 • The strain and the stress values in the crack development stage, which depend on the mechanical
54
55 properties of both the mortar and the textile, as well as on the textile-to-matrix bond/interlocking. These
56
57 parameters may affect the crack pattern and the composite-to-substrate performance and, therefore, the
58
59
60
61
62

effectiveness of the strengthening work for those structural applications in which the load is applied at the composite-to-substrate interface. Table 3 collects the tensile modulus of elasticity of the first two stages (E_I and E_{II}), as well as the strain and stress values of the transition points between stages I-II (ϵ_I , f_I), and II-III (ϵ_{II} , f_{II}) (Fig. 6).

- The crack width and distribution, which depend on the effectiveness of the textile-to-matrix stress transfer mechanism, and may affect durability against external aggression.

Figs. 8 and 9 show the results of tensile tests on composite specimens comprising glass-aramid and steel textiles, respectively, together with those of dry textiles. In glass-aramid composites (Fig. 8) cracking causes strong load reductions (derived thanks to the displacement control), which are clearly visible for the whole test duration (especially for G-ML and G-L series, Figs. 8c,d) and indicate that crack development (stage II) is the prevalent mechanism in these reinforcement systems. Both the average peak stress and the tensile modulus of elasticity are however close to those of the textile alone, while a decrease of the peak strain results, mainly for stronger and stiffer matrices (G-M and G-P series, Figs. 8a,b). Failure is always brittle and, due to the redistribution effect of the matrix, the difference in strength between glass and aramid yarns is less evident than in the dry textile. As regards steel composites, all the response curves are essentially superposed to those of the textiles (Fig. 9) as the crack widening stage (III) is prevalent with respect to the other mechanisms. The effect of the mortar is visible only in S4-C system, manufactured with the stronger mortar and the thinner textile (Fig. 9a). In this case the first two stages can be identified, while in all the other composites the contribution of the matrix is limited to a reduction of the peak strain in S4 specimens (Figs. 9a,b), especially when the stronger and stiffer mortar (C) is used, and to a reduction of the ultimate stress in S12 specimens (Figs. 9c,d). In this latter case, both a marked loss of linearity and instantaneous load reductions, caused by the rupture of one or few lateral cords, are seen in the response curves. Such a premature failure may be attributed to unavoidable non-uniform load distribution over the cross section of the textile, leading to strain/stress concentrations, especially in the vicinity of cracks, where the redistributing effect of the matrix vanishes. The outcome parameters of the first two stages present a higher scatter with respect to those of the last stage, due to the high variability of cracking phenomena, such that it is more difficult to identify clear relationships between the properties of the system and its response. As a general trend, the stiffer is the mortar, the higher are the tensile modulus of elasticity in the first stage and the stress of the transition point between stages I and II (f_I); a smaller E_{II}/E_I ratio is also found for stiffer matrices. The mean stress in the mortar has also been calculated before cracking and during crack development, dividing the load by the homogenised cross section of the composite specimen, in which the area of the textile is

1 amplified by the ratio between the tensile modulus of elasticity of the two materials. The resulting stress values
2 at the transition point between stages I and II (f_t) are always lower (between 15% and 60%) than the tensile
3 strength of the mortar (f_{mt}), especially for composites with the glass mesh (providing a weaker textile-to-matrix
4 load transfer capacity than steel cords), and for stronger matrices (e.g., cement instead of lime mortar). As it is
5 known, the three point bending tests may lead to an overestimate of the actual tensile strength, and, therefore, the
6 obtained f_{mt} cannot be considered a reliable prediction of f_t . Finally, the length of the crack development stage
7 can be represented by the ϵ_{II}/ϵ_t ratio (ϵ_t being the strain corresponding to the peak stress, as stated before). In
8 glass-aramid composites, ϵ_{II} is between 40% and 50% of the peak strain for G-M and G-P series and about 90%
9 for G-ML and G-L, indicating the predominance of the crack development stage. Conversely, ϵ_{II} is 29% of the
10 peak strain for S4-C, 2% and 5% for S4-ML and S12-C and, finally, not even detectable for S12-ML, in which
11 the contribution of the reinforcement fabric is largely prevalent with respect to that of the matrix, as already
12 found in [30] for TRC.
13
14
15
16
17
18
19
20
21
22
23
24
25

26 **3.3. Composite specimens: cyclic tests**

27
28 Cyclic tests have been performed on three G-M and three G-L specimens to provide hysteretic behaviour and
29 residual crack width development, and investigate the feasibility of the cyclic testing methodology itself. The
30 first unloading was performed immediately after the occurrence of the first crack, while the following cycles
31 were performed at about 0.05% strain increment. Load was reduced under displacement control at 0.01mm/s rate
32 to null force value. The response curves are shown in Fig. 10, together with those of the monotonic tests, which
33 generally appear superimposed to the cyclic ones, suggesting that the few cycles performed had scarce influence
34 on overall stiffness and bearing capacity (similarly to what was found for TRC in [31]). After each unloading
35 phase, the residual average crack width was derived as the residual displacement (at zero load) divided by the
36 number of cracks, as shown in Figs. 10c,d. Clearly, an increase in the number of cracks during test execution is
37 associated with an increase of the overall amount of irreversible deformation, even if it may result in a decrease
38 of the average residual crack width, the latter being referred to a single crack. In the specimens with mineral
39 mortar (G-M, Figs. 10a,c), 4 cracks developed, the width of the first crack was between 0.45mm and 0.6mm,
40 while the final average crack width was between 0.4mm and 0.52mm. Differently, the specimens with lime
41 mortar (G-L, Figs. 10b,d) showed 6 cracks, the first crack width was between 0.08mm and 0.18mm and, finally,
42 the final average crack width was between 0.22mm and 0.3mm. The tests indicate that a stiffer matrix may lead
43 to larger cracks, especially in stage II, because of both the higher strain of the first transition point (ϵ_I , see Table
44
45
46
47
48
49
50
51
52
53
54
55
56
57
58
59
60
61
62
63
64
65

3), and the smaller number of cracks. Despite the need for wider investigation, the results of cyclic tests suggest that stiffer matrices, compared to more deformable ones, provide a worse reinforcement-to-substrate load transfer, leading to wider cracks under cyclic loading. Thereby, the textile is expected to be more exposed to the external aggression, threatening the durability of the strengthening work and the long term protection of the structure.

4. COMPARISONS

4.1. Peak stress and tensile modulus of elasticity

The peak stress and the tensile modulus of elasticity of all the composite specimens are plotted in Figs. 11a and 11b, and compared to those of the textiles. Round marks represent glass-aramid systems, while triangle and squared marks stand for S4 and S12 composites, respectively. As for the former ones, despite a certain variability amongst the four series, both the strength and the stiffness are very close to those of the dry glass-aramid textile, indicating that the ultimate mechanical properties mainly depend on the characteristics of the textile. Conversely, steel composites resulted slightly weaker than the textiles, with the only exception of S4-ML series. Such strength reduction is higher for the stronger mortar (C instead of ML matrix) and for the stiffer textile (S12 instead of S4), similarly to previous findings on TRC [21,29], and is likely to be due to a non-uniform stress distribution amongst the cords, concentrated in a short length over one or more cracked sections, where no redistribution is offered by the matrix. As discussed beforehand, such stress concentration may be also responsible for the pronounced loss of linearity in the stress-strain curves (which appears earlier in composite than in textile specimens) and the premature rupture of some lateral cords (identifiable by the small but instantaneous losses of load).

4.2. Crack pattern

The crack pattern is affected by the layout of the textile (influencing the bond/interlocking with the matrix) and the Young's modulus of the mortar. The average saturation crack spacing (δ), i.e., the distance between cracks in stage III, is plotted in Fig. 12 versus the Young's modulus of the mortar, while the crack pattern in the last stage is depicted in Fig. 13. The textile being equal, less cracks at larger distances develop for matrices with higher tensile modulus of elasticity (G-M, S4-C, and S12-C series). Furthermore, the better is the bond/interlocking (as in steel-based composites), the shorter is the saturation crack spacing (smaller and more distributed cracks

1 develop). Slight differences amongst steel-based systems are seen, which depend either on the layout of the
2 textiles, or on the properties of the matrix. More specifically, in S12-ML series the saturation crack spacing is
3 lower than in S4-ML, similarly to reinforced concrete members under bending, in which a higher reinforcement
4 ratio is related to a shorter distance between cracks. Differently, a larger saturation crack spacing is found in
5 S12-C specimens than in S12-ML, which may be related to a worse penetration of the cement mortar, having a
6 higher grain size range and comprising microfibres (Table 1). As a result, a splitting failure mode occurs (Fig.
7 13), characterized by the separation of the specimen into two halves and the expulsion of large portions of
8 mortar.
9

10 The stress-strain curves evaluated by the LVDT, the potentiometers and the extensometer (Fig. 2) for two
11 different composite specimens are plotted in Fig. 14, to provide information on the reliability of
12 displacement/strain measurements related to crack pattern and gripping method. A good agreement is found for
13 the whole test duration between the measurements of the LVDT (recording the overall displacement from end
14 plate to end plate) and those of the potentiometers (applied to the mortar matrix and recording the relative
15 displacement within a measurement base of about 250mm), confirming that no slipping occurs in the gripping
16 areas. Differently, the strain recorded by the extensometer appears reliable in the un-cracked stage, but not in the
17 following part of the tests, especially when few cracks develop, as in glass-aramid G-M series. In this specific
18 case, two cracks formed at a distance of 162mm, and one of them occurred within the 50mm measurement base
19 of the device, such that its progressive widening during stages II and III resulted in overestimated strain
20 recordings (Fig. 14a). In the S4-C specimen represented in Fig. 14b, seven cracks formed at an average distance
21 of 41mm, and one of them occurred within the measurement base of the extensometer. As a consequence, the
22 three curves are closer than in G-M series, despite a slight overestimate of the tensile modulus of elasticity in
23 stage III.
24
25
26
27
28
29
30
31
32
33
34
35
36
37
38
39
40
41
42
43
44
45

46 **4.3. Failure mode**

47 The failure mode is mainly governed by the reinforcement fabric. In glass-aramid composites, failure generally
48 occurs in a cross section comprising a yarn perpendicular to the load direction, providing an increased anchorage
49 [22], but also a reduction of the mortar section, which becomes a preferential weak location for crack
50 development and textile sliding (Fig. 15a). The roving failure mechanism is initiated by the rupture of the outer
51 filament ring, followed by that of the adjacent layers until reaching the core filaments (Fig. 15b), which are not
52 directly connected to the matrix. Such telescopic failure is likely to be due to the weaker bond between filaments
53
54
55
56
57
58
59
60
61
62
63
64
65

1 than that between outer filaments and mortar [30]. Differently, in steel composites, no sliding of the cords within
2 the matrix occurs (Fig. 15c) and, clearly, no telescopic failure develops as steel cords are not made out of wire
3 bundles. As already said, failure is preceded by a clear loss of linearity in the stress-strain response curve (Fig. 9)
4 and, generally, by the rupture of one or few lateral cords. Finally, the recovery of cords' elastic strain after
5 rupture may cause the expulsion of mortar portions (Fig. 15d).
6
7
8
9

10 11 **5. CONCLUSIONS**

12 Direct tensile tests have been carried out on eight types of mortar-based reinforcements comprising two textiles
13 and five matrices, to gain an improved knowledge on their mechanical properties and contribute to the definition
14 of appropriate testing methodologies. The main conclusions can be summarized as follows:
15
16
17

- 18 • The ultimate strength, the tensile modulus of elasticity in the cracked stage and the failure mode are
19 mainly governed by the properties of the textile. Nevertheless, due to the stiffening effect of the mortar,
20 the peak strain is often lower than that of the dry textiles. The composites with good textile-to-matrix
21 interlocking also display a slight reduction of the stiffness and of the maximum attainable stress which
22 may depend on stress concentrations in the cracked sections.
23
- 24 • The contribution of the mortar in the first stages (un-cracked and crack development) is prevalent in
25 composites with relatively weak and deformable fabrics (e.g., glass-aramid mesh), while it may be
26 nearly negligible when the strength and the stiffness of the textile are much higher than those of the
27 mortar (e.g., thick steel textile and lime mortar).
28
- 29 • Stronger and stiffer matrices (e.g., cement instead of lime mortars) lead to a higher stiffness in both the
30 un-cracked and cracked stages and to a larger saturation crack spacing. At the same time, textiles
31 providing better interlocking with the matrix (e.g., steel cords) entail better crack distribution with
32 respect to those with poor textile-to-mortar bond (e.g., glass-aramid mesh). In the former ones, crack
33 widening is the dominant mechanism, while crack development is prevalent in the latter ones.
34
- 35 • Cyclic tests require a much longer runtime than monotonic tests, but provide some information on
36 hysteretic behaviour and crack development. The higher are the stiffness and the strength of the matrix,
37 the larger is the average residual crack width, especially at low strain values, due to the smaller number
38 of cracks and to the higher strain at which the first crack occurs.
39

40 Different testing setups have been experimented, leading to the following conclusions on gripping mechanism
41 and displacement/strain measurement:
42
43
44
45
46
47
48
49
50
51
52
53
54
55

- Clamping mortar-based composites directly on the mortar allows for an appropriate load application to the whole specimen, and for the full characterization of the strengthening system under tension. The ends of the specimen need to be reinforced to prevent mortar crushing, while pull-out effects and sliding in the gripping areas can be avoided by applying an adequate transversal load.
- Specimens with sufficient textile-to-mortar bond/interlocking (e.g., those with steel cords) are scarcely sensitive to the gripping mechanism, provided that premature ripping of the textile is avoided in the gripping areas. Clamping can be made either directly on the mortar or, as an effective alternative, on the textile, left free of mortar, by means of aluminium tabs glued with a strong adhesive.
- Global strain measurements acquired from end plate to end plate are reliable provided that sliding is avoided in the gripping areas. Local strains and displacements recorded after cracking by devices applied on the mortar are sufficiently accurate if the measurement base is large with respect to the saturation crack spacing, such that the recordings are not influenced by the number and location of cracks.

Due to the large variability of textiles and matrices, the results derived in this study cannot be directly extrapolated to different mortar-based composites, but each specific strengthening system needs to be characterized. In addition to tensile behaviour, other fundamental parameters are needed for strengthening design and product qualification purposes, such as the composite-to-substrate shear bond performance, which determines the effectiveness of the installation, and the durability performance of both dry reinforcement textiles and strengthening composites, which ensures the long term protection of reinforced structures.

ACKNOWLEDGEMENTS

The work has been carried out with the financial support of the research projects “MIUR PRIN-2009, Analysis and Modelling Strategies for the Conservation of multi-leaf Historical Masonry” and “ReLUIS-DPC 2010-2013, Thematic Area 1 - Seismic assessment of built heritage, Task 1.1 - Masonry structures and cultural heritage” and of the research agreement with Kerakoll S.p.A. (signed 25 March 2013). The technical cooperation of Dr. Paolo Casadei is kindly acknowledged.

REFERENCES

- [1] Papanicolaou CG, Triantafyllou TC, Karlos K, Papathanasiou M. Textile reinforced mortar (TRM) versus FRP as strengthening material of URM walls: in-plane cyclic loading. RILEM Mater Struct 2007;40(10):1081-1097.

- 1
2
3
4
5
6
7
8
9
10
11
12
13
14
15
16
17
18
19
20
21
22
23
24
25
26
27
28
29
30
31
32
33
34
35
36
37
38
39
40
41
42
43
44
45
46
47
48
49
50
51
52
53
54
55
56
57
58
59
60
61
62
63
64
65
- [2] de Felice G, De Santis S, Garmendia L, Ghiassi B, Larrinaga P, Lourenço PB, Oliveira DV, Paolacci F, Papanicolaou CG. Mortar-based systems for externally bonded strengthening of masonry. *RILEM Mater Struct* 2014. DOI: 10.1617/s11527-014-0360-1.
 - [3] Valluzzi MR, Modena C, de Felice G. Current practice and open issues in strengthening historical buildings with composites. *RILEM Mater Struct* 2014. DOI: 10.1617/s11527-014-0359-7.
 - [4] Ascione L, Feo L, Fraternali F. Load carrying capacity of 2D FRP/strengthened masonry structures. *Compos Part B-Eng* 2005;36(8):619-626.
 - [5] Valluzzi MR, Oliveira DV, Caratelli A, Castori G, Corradi M, de Felice G, Garbin E, Garcia D, Garmendia L, Grande E, Ianniruberto U, Kwiecień A, Leone M, Lignola GP, Lourenço PB, Malena M, Micelli F, Panizza M, Papanicolaou CG, Prota A, Sacco E, Triantafillou TC, Viskovic A, Zając B, Zuccarino G. Round Robin test for composite-to-brick shear bond characterization. *RILEM Mater Struct* 2012;45(12):1761-1791.
 - [6] Carbone I, de Felice G. Debonding of CTRM composite on masonry support. In: *Proceedings of Prohitec09, Int Conf on Protection of Historical Buildings, Rome, Italy, 2009.*
 - [7] D'Ambrisi A, Feo L, Focacci F. Experimental analysis on bond between PBO-FRCM strengthening materials and concrete. *Compos Part B-Eng* 2013;44(1):524-532.
 - [8] D'Ambrisi A, Feo L, Focacci F. Experimental and analytical investigation on bond between Carbon-FRCM materials and masonry. *Compos Part B-Eng* 2013;46:15-20.
 - [9] Carozzi FG, Milani G, Poggi C. Mechanical properties and numerical modeling of Fabric Reinforced Cementitious Matrix (FRCM) systems for strengthening of masonry structures. *Compos Struct* 2014;107:711-725.
 - [10] Malena M, de Felice G. Externally bonded composites on a curved masonry substrate. *Compos Struct* 2014;112:194-206.
 - [11] D'Antino T, Carloni C, Sneed LH, Pellegrino C. Matrix-fiber bond behavior in PBO FRCM composites: a fracture mechanics approach. *Eng Fract Mech* 2014;117:94-111.
 - [12] Garmendia L, San-José JT, García D, Larrinaga P. Rehabilitation of masonry arches with compatible advanced composite material. *Constr Build Mater* 2011;25(12):4374-4385.
 - [13] Parisi F, Iovinella I, Balsamo A, Augenti N, Prota A. In-plane behaviour of tuff masonry strengthened with inorganic matrix-grid composites. *Compos Part B-Eng* 2013;45(1):1657-1666.

- 1
2
3
4
5
6
7
8
9
10
11
12
13
14
15
16
17
18
19
20
21
22
23
24
25
26
27
28
29
30
31
32
33
34
35
36
37
38
39
40
41
42
43
44
45
46
47
48
49
50
51
52
53
54
55
56
57
58
59
60
61
62
63
64
65
- [14] De Caso F, Matta F, Nanni A. Fiber reinforced cement-based composite system for concrete confinement. *Constr Build Mater* 2012;32:55-65.
- [15] D'Ambrisi A, Focacci F. Flexural strengthening of RC beams with cement-based composites. *J Compos Constr* 2011;15(5):707-720.
- [16] Borri A, Castori G, Corradi M. Shear behavior of masonry panels strengthened by high strength steel cords. *Constr Build Mater* 2011;25(2):494-503.
- [17] Triantafillou TC, Papanicolaou CG. Innovative applications of textile-based composites in strengthening and seismic retrofitting as well as in the prefabrication of new structures. *Adv Mater Res* 2013;639-640(1):26-41.
- [18] CNR. CNR-DT 200 R1/2012. Guide for the Design and Construction of Externally Bonded FRP Systems for Strengthening Existing Structures. Italian Research Council, Italy, 2012.
- [19] ICC. AC434. Proposed acceptance criteria for masonry and concrete strengthening using fiber-reinforced cementitious matrix (FRCM) composite systems. ICC-Evaluation Service, Whittier, CA, 2013.
- [20] Brameshuber W. Textile reinforced concrete. State-of-the-art report of RILEM Technical Committee 201-TRC. Report 36, Bagnaux, RILEM, 2006.
- [21] Hegger J, Will N, Bruckermann O, Voss S. Load-bearing behaviour and simulation of textile reinforced concrete. *RILEM Mater Struct* 2006;39(8):765-776.
- [22] Colombo IG, Magri A, Zani G, Colombo M, di Prisco M. Textile Reinforced Concrete: experimental investigation on design parameters. *RILEM Mater Struct* 2013;46(11):1933-1951.
- [23] Contamine R, Si Larbi A, Hamelin P. Contribution to direct tensile testing of textile reinforced concrete (TRC) composites. *Mater Sci Eng A* 2011;528(29-30):8589-8598.
- [24] Hartig J, Jesse F, Schicktanz K, Häußler-Combe U. Influence of experimental setups on the apparent uniaxial tensile load-bearing capacity of Textile Reinforced Concrete specimens. *RILEM Mater Struct* 2012;45(3):433-446.
- [25] Balsamo A, Di Ludovico M, Prota A, Manfredi G. Masonry walls strengthened with innovative composites. *American Concr Inst, ACI Spec Publ* 2011;2(275):769-786.
- [26] Pacheco-Torgal F, Jalali S. Cementitious building materials reinforced with vegetable fibres: A review. *Constr Build Mater* 2011;25(2):575-581.
- [27] CEN EN 1015-2:1998. Methods of test for mortar for masonry - Part 2: Bulk sampling of mortars and preparation of test mortars. Brussels, B, 1998.

- 1
2
3
4
5
6
7
8
9
10
11
12
13
14
15
16
17
18
19
20
21
22
23
24
25
26
27
28
29
30
31
32
33
34
35
36
37
38
39
40
41
42
43
44
45
46
47
48
49
50
51
52
53
54
55
56
57
58
59
60
61
62
63
64
65
- [28] CEN EN 196-1:2005. Methods of testing cement - Part 1: Determination of strength. Brussels, B, 2005.
- [29] Häußler-Combe U, Hartig J. Bond and failure mechanisms of textile reinforced concrete (TRC) under uniaxial tensile loading. *Cem Concr Compos* 2007;29(4):279-289.
- [30] Mobasher B, Peled A, Pahilajani J. Distributed cracking and stiffness degradation in fabric-cement composites. *RILEM Mater Struct* 2006;39(3):317-331.
- [31] Hegger J, Voss S. Investigations on the bearing behaviour and application potential of textile reinforced concrete. *Eng Struct* 2008;30(7):2050-2056.

1
2
3
4
5
6
7
8
9
10
11
12
13
14

LIST OF TABLE CAPTIONS

Table 1. Composite specimens for monotonic tensile tests and mechanical properties of mortar matrices.

Table 2. Results of tensile tests on textile and composite specimens: peak stress, peak load per unit width, peak strain and tensile modulus of elasticity in stage III (Coefficients of Variation in round brackets).

Table 3. Results of tensile tests on composite specimens: transition points and tensile modulus of elasticity in stages I and II (Coefficients of Variation in round brackets).

15
16
17

LIST OF FIGURE CAPTIONS

Figure 1. Reinforcement fabric types: unbalanced bidirectional glass-aramid mesh (a), unidirectional UHTSS textile with 4 cords/inch (b) and 12 cords/inch (c).

Figure 2. Testing setup for textile (a) and composite (b) specimens.

Figure 3. Clamping methods (a, c, e, g, i) and their effect on test execution and results (b, d, f, h, j).

Figure 4. Effect of the clamping method on the stress-strain response of composite specimens (G-M series).

Figure 5. Stress-strain response curves of fabric specimens: glass-aramid mesh (a) and steel textiles (b).

Figure 6. Characteristic stress-strain response curve of composite specimens (clamping method CM-5).

Figure 7. Crack pattern evolution: first crack occurrence (a), crack development (b), expulsion of mortar fragments (c), failure (d).

Figure 8. Stress-strain response curves of composite specimens with glass-aramid mesh and mineral mortar (G-M series, a), polymer-modified cement mortar (G-P series), mineral NHL mortar (G-ML series, c) and NHL mortar (G-L series, d) (clamping method CM-3).

Figure 9. Stress-strain response curves of composite specimens with steel textiles: 4 cords/inch textile with cement mortar (S4-C series, a) and mineral NHL mortar (S4-ML series, b), 12 cords/inch textile with cement mortar (S12-C series, c) and mineral NHL mortar (S12-ML series, d) (clamping method CM-5).

Figure 10. Cyclic tests on G-L (a, c) and G-M (b, d) series: stress-strain response curves (a, b) and average residual crack width vs. residual strain (c, d) (clamping method CM-5).

Figure 11. Comparisons between textile and composite specimens: tensile strength (a) and tensile modulus of elasticity (b).

Figure 12. Saturation crack spacing vs. mortar Young's modulus.

Figure 13. Crack pattern in composite specimens.

Figure 14. Comparison between different devices for displacement/strain measurement in G-M (a) and S4-C (b) specimens.

Figure 15. Failure mode in composite specimens with glass-aramid mesh (a, b) and steel cords (c, d).

Table 2

| Specimen | | Equivalent thickness t [mm] | Tensile strength (peak stress) f_t [N/mm ²] | Tensile strength (per unit width) F_t [N/mm] | Peak strain (at peak stress) ϵ_t [%] | Young's modulus Tensile modulus of elasticity (Stage III) E_{III} [kN/mm ²] |
|-----------|--------|--------------------------------|---|--|---|---|
| Textile | G | 0.030 | 1829.3 (7.2%) | 55.2 | 2.15 (7.5%) | 101.5 (4.3%) |
| Composite | G-M | | 1859.2 (5.0%) | 56.0 | 1.68 (15.9%) | 109.9 (8.9%) |
| | G-P | | 1875.5 (5.5%) | 56.9 | 1.73 (16.6%) | 96.9 (3.8%) |
| | G-ML | | 1977.2 (4.5%) | 59.3 | 1.89 (14.2%) | 105.1 (6.9%) |
| | G-L | | 1835.4 (4.8%) | 55.2 | 1.92 (10.4%) | 108.0 (3.5%) |
| Textile | S4 | 0.084 | 3207.7 (0.7%) | 269.1 | 2.24 (3.8%) | 183.9 (6.0%) |
| Composite | S4-C | | 3027.8 (2.8%) | 254.1 | 1.65 (8.8%) | 177.3 (2.6%) |
| | S4-ML | | 3245.3 (2.8%) | 279.5 | 2.15 (6.3%) | 182.9 (2.6%) |
| Textile | S12 | 0.254 | 3082.6 (1.6%) | 783.0 | 2.20 (4.6%) | 183.3 (4.3%) |
| Composite | S12-C | | 2852.5 (5.1%) | 724.0 | 2.15 (9.9%) | 173.5 (4.0%) |
| | S12-ML | | 2804.1 (5.1%) | 712.8 | 2.18 (11.1%) | 178.7 (2.8%) |

1
2
3
4
5
6
7
8
9
10
11
12
13
14
15
16
17
18
19
20
21
22
23
24
25
26
27
28
29
30
31
32
33
34
35
36
37
38
39
40
41
42
43
44
45
46
47
48
49
50
51
52
53
54
55
56
57
58
59
60
61
62
63
64
65

Table 3

| Composite Specimen | Young's modulus Tensile modulus of elasticity (Stage I) E_I [kN/mm ²] | Transition point between stages I-II | | Young's modulus Tensile modulus of elasticity (Stage II) E_{II} [kN/mm ²] | Transition point between stages II-III | |
|--------------------|--|--------------------------------------|-------------------------|--|--|----------------------------|
| | | Stress f_I [N/mm ²] | Strain ϵ_I [%] | | Stress f_{II} [N/mm ²] | Strain ϵ_{II} [%] |
| G-M | 416.2 (16.4%) | 577 (34.4%) | 0.15 (44.7%) | 48.9 (28.2%) | 867 (19.8%) | 0.75 (46.8%) |
| G-P | 404.0 (21.2%) | 761 (16.9%) | 0.21 (34.6%) | 16.5 (24.2%) | 841 (13.1%) | 0.71 (16.8%) |
| G-ML | 263.2 (13.5%) | 605 (24.5%) | 0.27 (46.1%) | 71.5 (22.8%) | 1233 (18.1%) | 1.72 (23.3%) |
| G-L | 343.6 (25.0%) | 468 (24.2%) | 0.13 (20.2%) | 54.5 (36.3%) | 891 (29.1%) | 1.69 (24.8%) |
| S4-C | 1059.2 (3.8%) | 498 (8.8%) | 0.05 (13.9%) | 108.1 (13.9%) | 965 (23.9%) | 0.48 (9.0%) |
| S4-ML | 292.6 (22.7%) | 121 (9.4%) | 0.05 (19.8%) | 120.9 (16%) | 205 (6.9%) | 0.05 (7.7%) |
| S12-C | 376.6 (26.4%) | 130 (24.2%) | 0.04 (34.7%) | 56.7 (14%) | 181 (11.5%) | 0.11 (18.8%) |
| S12-ML | Undetectable | Undetectable | Undetectable | Undetectable | Undetectable | Undetectable |

1
2
3
4
5
6
7
8
9
10
11
12
13
14
15
16
17
18
19
20
21
22
23
24
25
26
27
28
29
30
31
32
33
34
35
36
37
38
39
40
41
42
43
44
45
46
47
48
49
50
51
52
53
54
55
56
57
58
59
60
61
62
63
64
65

Table 1

| Textile | Mortar matrix | | | | | Composite acronym |
|--|-----------------------------|----------------------------------|-----------------------------------|----------------------------------|-----------|-------------------|
| | Type | f_{mc} [N/mm ²] | E_{mc} [kN/mm ²] | f_{mt} [N/mm ²] | D [mm] | |
| Unbalanced bi-directional glass-aramid fabric (warp direction) [G] | Mineral [M] | 56.3 | 22.0 | 10.3 | 0÷0.5 | G-M |
| | Polymer-modified cement [P] | 22.8 | 10.3 | 6.9 | 0.5÷0.6 | G-P |
| | Mineral NHL [ML] | 20.6 | 11.4 | 5.4 | 0÷1.4 | G-ML |
| | NHL [L] | 12.3 | 10.9 | 4.4 | 0÷1.5 | G-L |
| Unidirectional galvanized UHTSS cords (4 cords/inch) [S4] | Cement [C] | 49.0 | 31.5 | 5.5 | 0.3÷3.0 | S4-C |
| | Mineral NHL [ML] | 20.6 | 11.4 | 5.4 | 0÷1.4 | S4-ML |
| Unidirectional galvanized UHTSS cords (12 cords/inch) [S12] | Cement [C] | 49.0 | 31.5 | 5.5 | 0.3÷3.0 | S12-C |
| | Mineral NHL [ML] | 20.6 | 11.4 | 5.4 | 0÷1.4 | S12-ML |

Table 2

| Specimen | | Equivalent thickness t [mm] | Tensile strength (peak stress) f_t [N/mm ²] | Tensile strength (per unit width) F_t [N/mm] | Peak strain (at peak stress) ε_t [%] | Tensile modulus of elasticity (Stage III) E_{III} [kN/mm ²] |
|-----------|--------|--------------------------------|---|--|--|---|
| Textile | G | 0.030 | 1829.3 (7.2%) | 55.2 | 2.15 (7.5%) | 101.5 (4.3%) |
| Composite | G-M | | 1859.2 (5.0%) | 56.0 | 1.68 (15.9%) | 109.9 (8.9%) |
| | G-P | | 1875.5 (5.5%) | 56.9 | 1.73 (16.6%) | 96.9 (3.8%) |
| | G-ML | | 1977.2 (4.5%) | 59.3 | 1.89 (14.2%) | 105.1 (6.9%) |
| | G-L | | 1835.4 (4.8%) | 55.2 | 1.92 (10.4%) | 108.0 (3.5%) |
| Textile | S4 | 0.084 | 3207.7 (0.7%) | 269.1 | 2.24 (3.8%) | 183.9 (6.0%) |
| Composite | S4-C | | 3027.8 (2.8%) | 254.1 | 1.65 (8.8%) | 177.3 (2.6%) |
| | S4-ML | | 3245.3 (2.8%) | 279.5 | 2.15 (6.3%) | 182.9 (2.6%) |
| Textile | S12 | 0.254 | 3082.6 (1.6%) | 783.0 | 2.20 (4.6%) | 183.3 (4.3%) |
| Composite | S12-C | | 2852.5 (5.1%) | 724.0 | 2.15 (9.9%) | 173.5 (4.0%) |
| | S12-ML | | 2804.1 (5.1%) | 712.8 | 2.18 (11.1%) | 178.7 (2.8%) |

Figure 1
[Click here to download high resolution image](#)

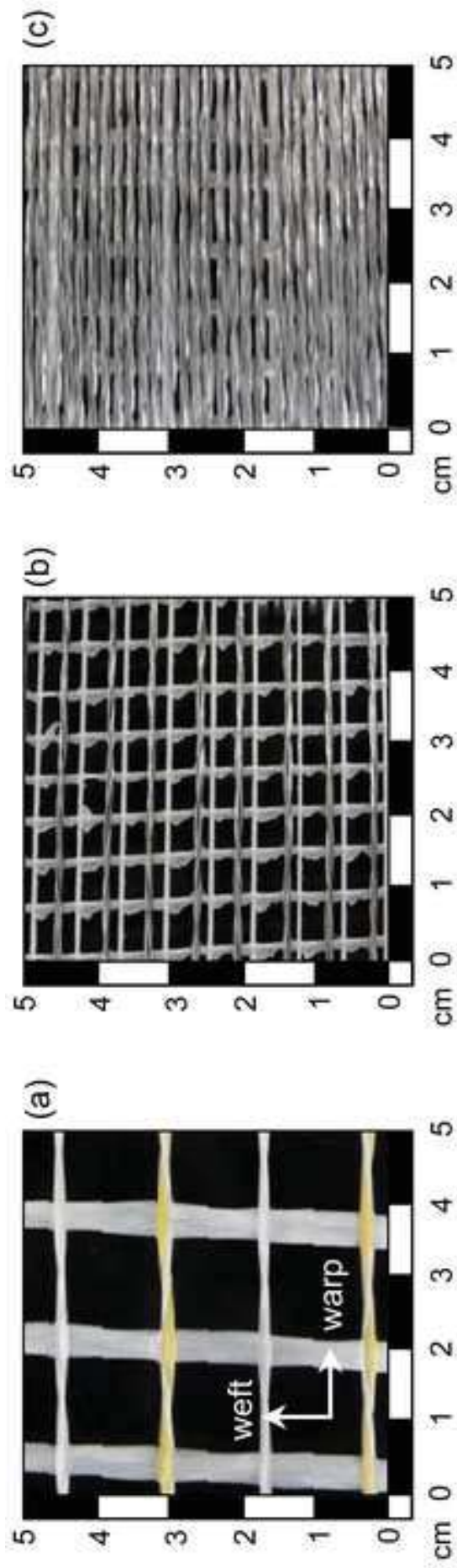


Figure 2
Click here to download high resolution image

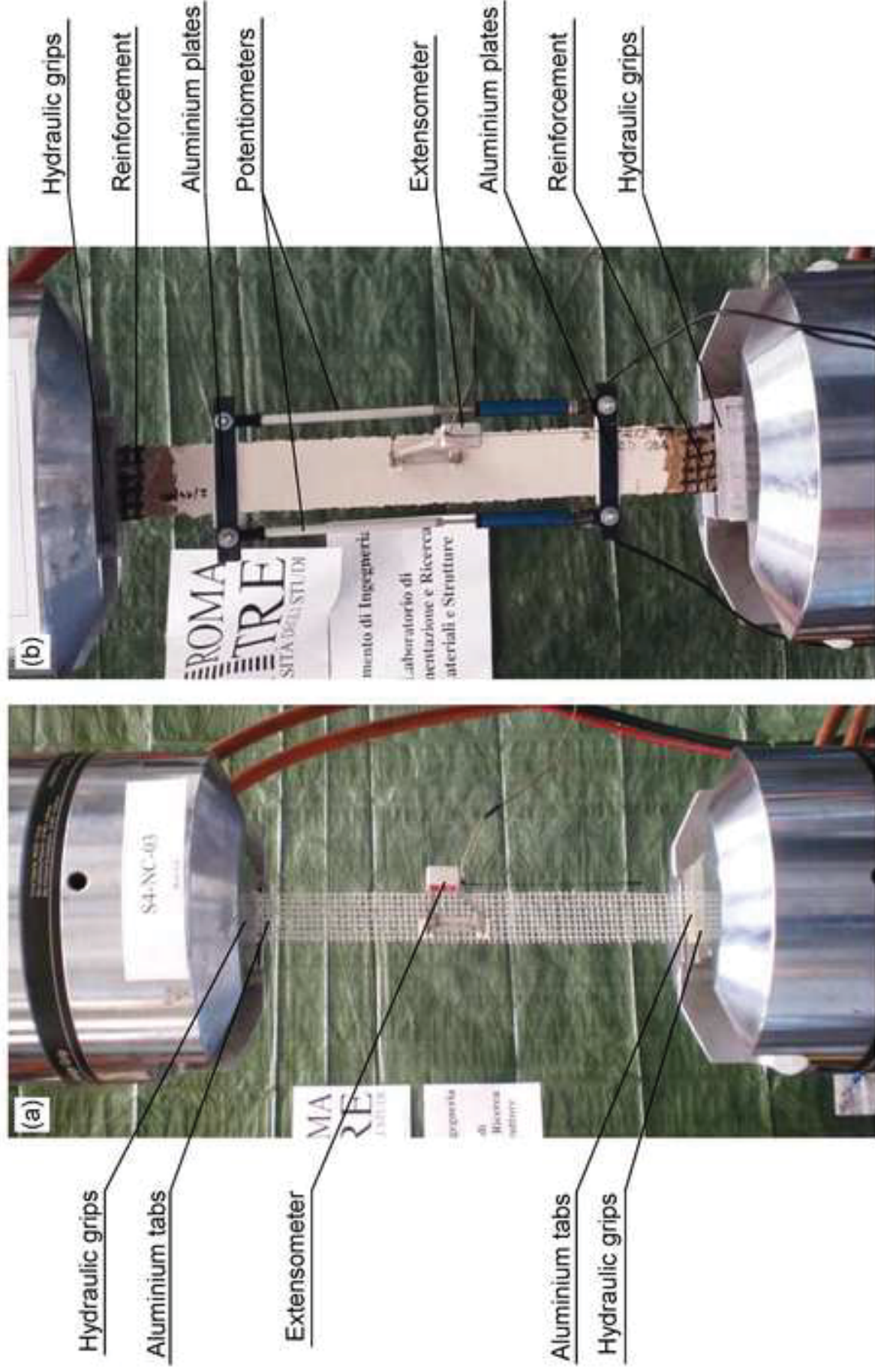
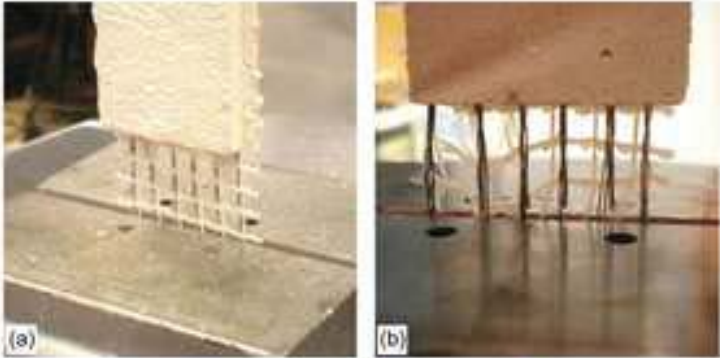
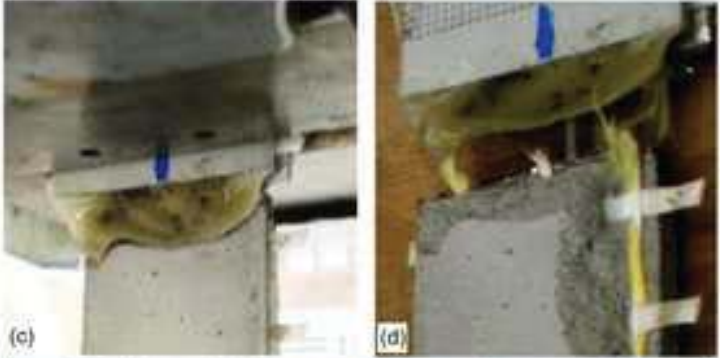


Figure 3
[Click here to download high resolution image](#)

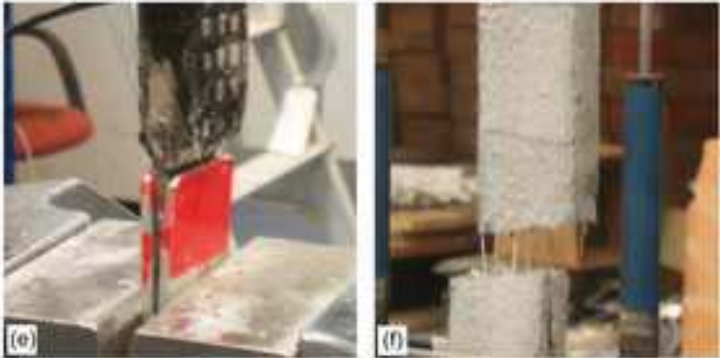
Clamping Method CM-1
Direct clamping of reinforcement textile (specimen ends free of mortar)
↓
Textile rupture at the edge of the grip



Clamping Method CM-2
Aluminium tabs glued to the specimen ends (free of mortar)
↓
Textile rupture at the beginning of mortar matrix



Clamping Method CM-3
Aluminium tabs glued to the specimen ends (free of mortar), reinforced with FRP
↓
Satisfactory crack pattern and failure mode



Clamping Method CM-4
Spherical articulation and aluminium tabs glued to the mortar matrix
↓
Sliding of the textile within the mortar matrix



Clamping Method CM-5
Direct clamping on the mortar matrix, reinforced with FRP
↓
Satisfactory crack pattern and failure mode

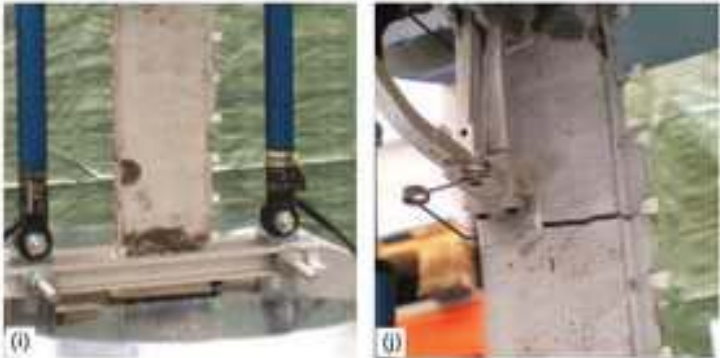


Figure 4 new
[Click here to download high resolution image](#)

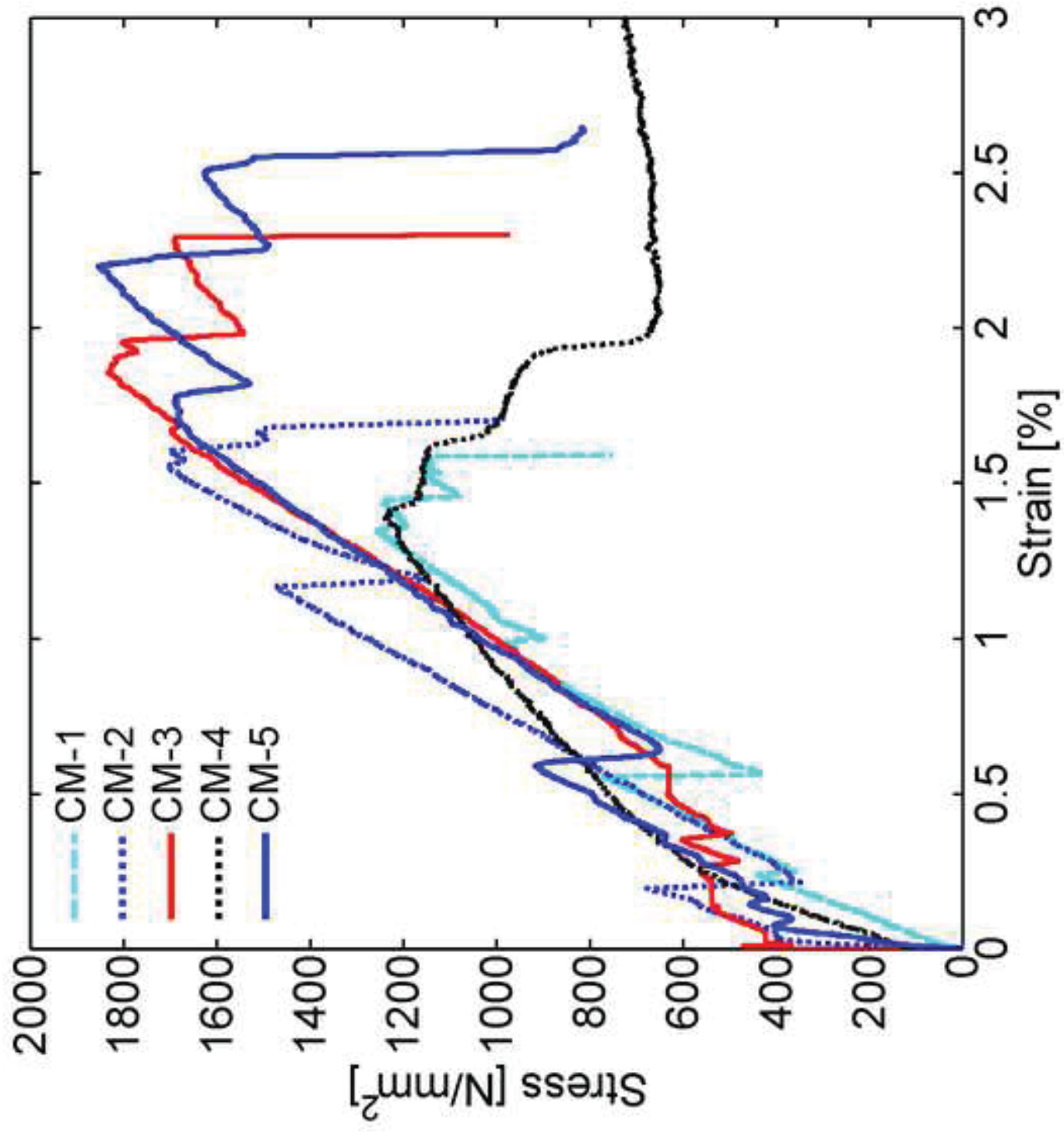


Figure 5
[Click here to download high resolution image](#)

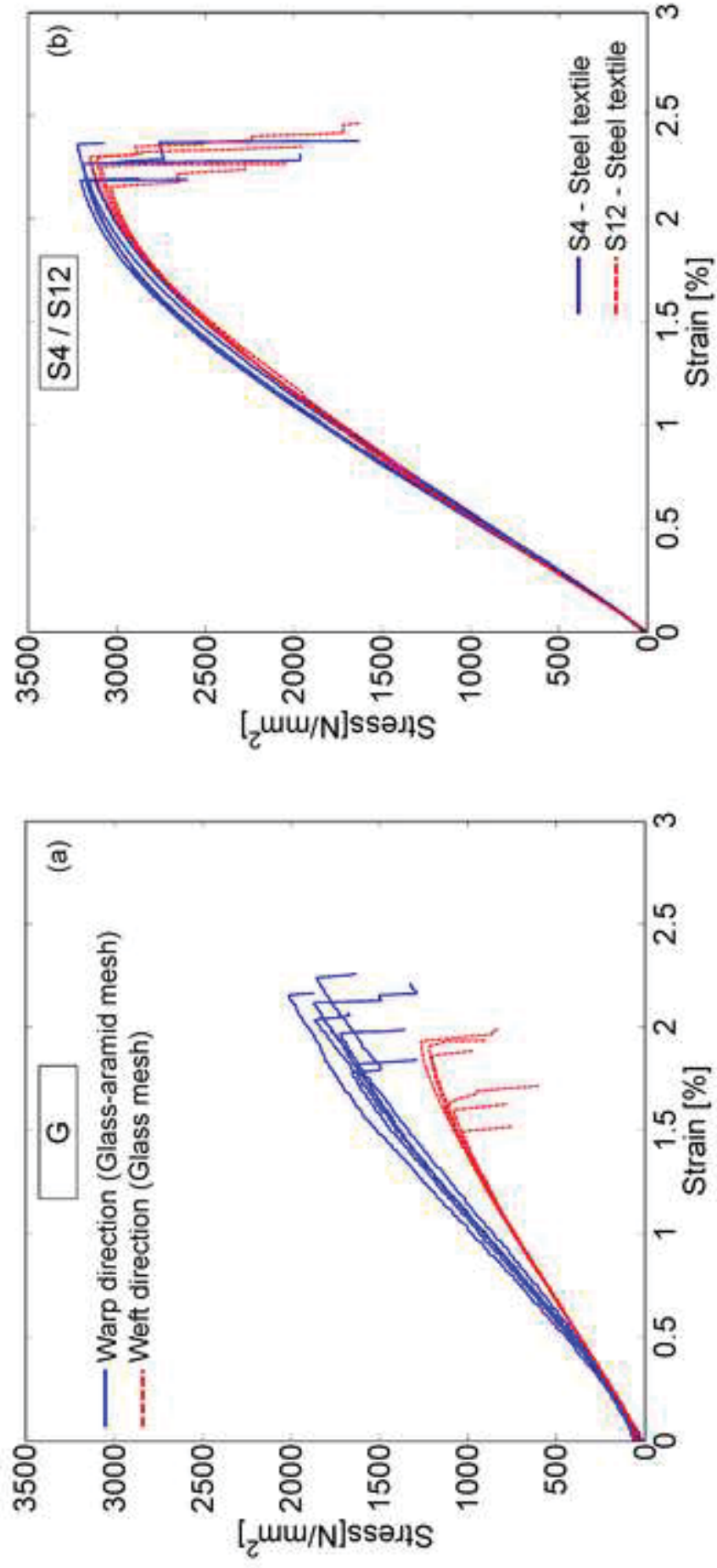
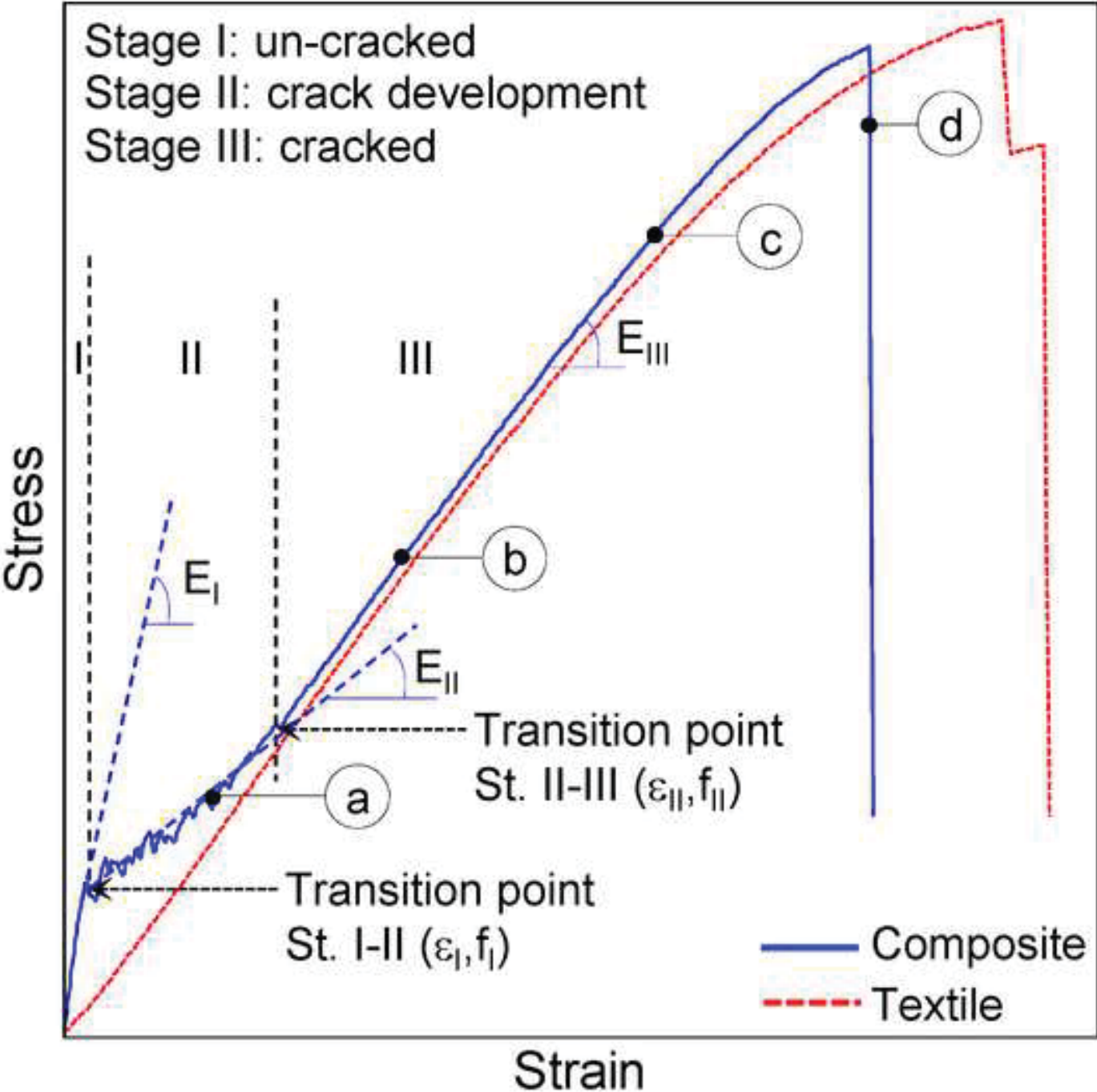


Figure 6
[Click here to download high resolution image](#)



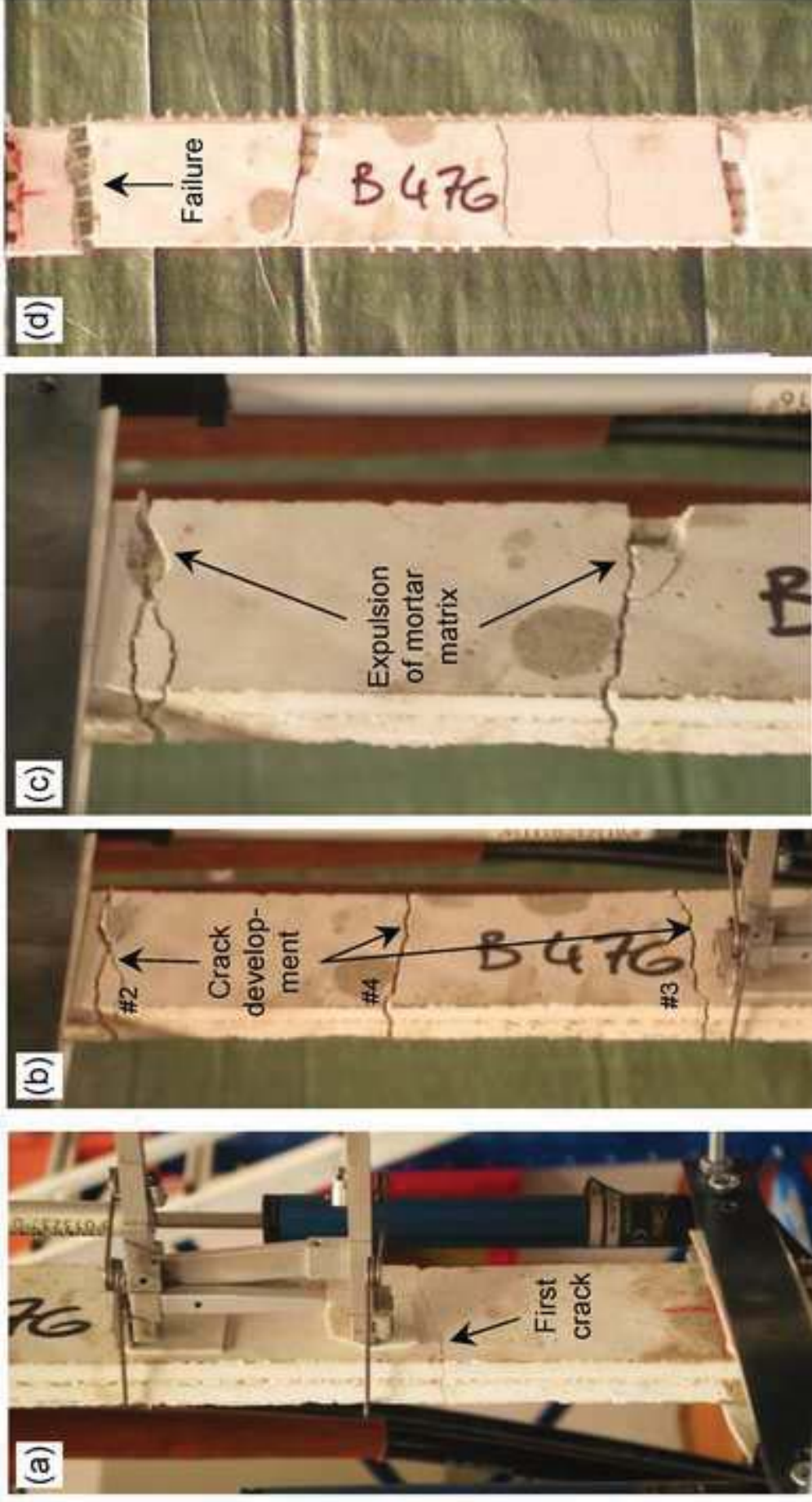


Figure 7
[Click here to download high resolution image](#)

Figure 8
[Click here to download high resolution image](#)

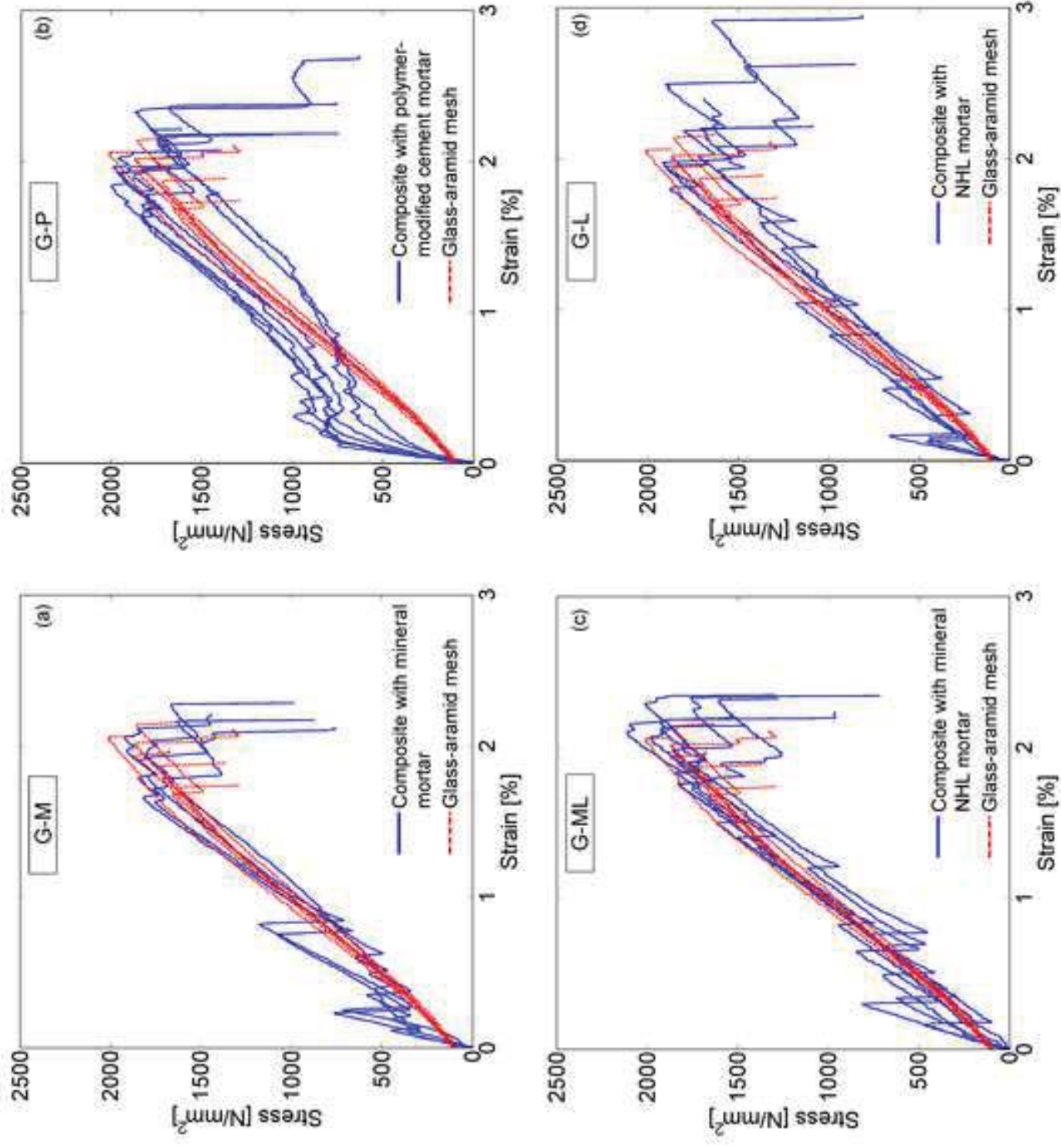


Figure 9
[Click here to download high resolution image](#)

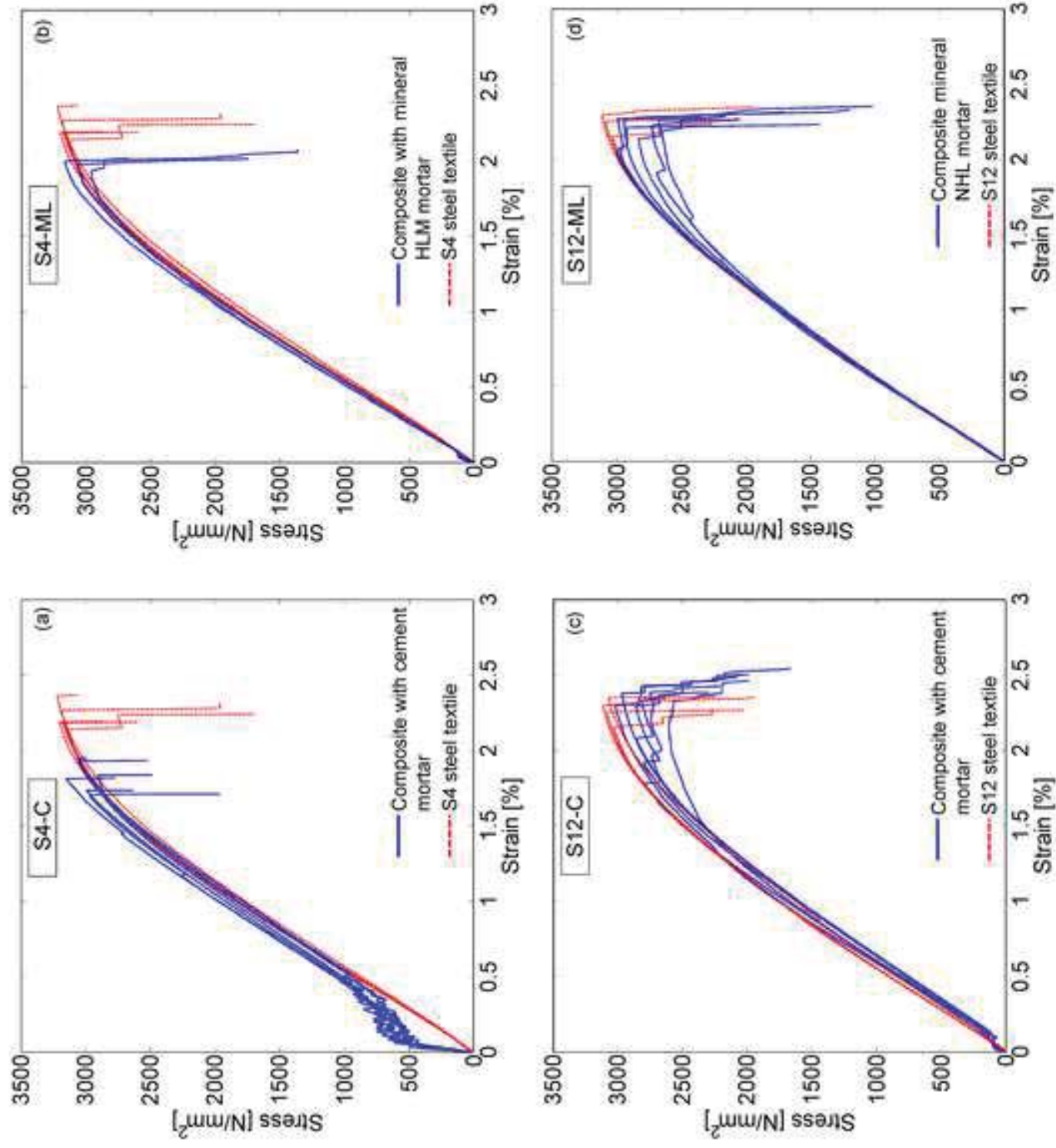


Figure 10
[Click here to download high resolution image](#)

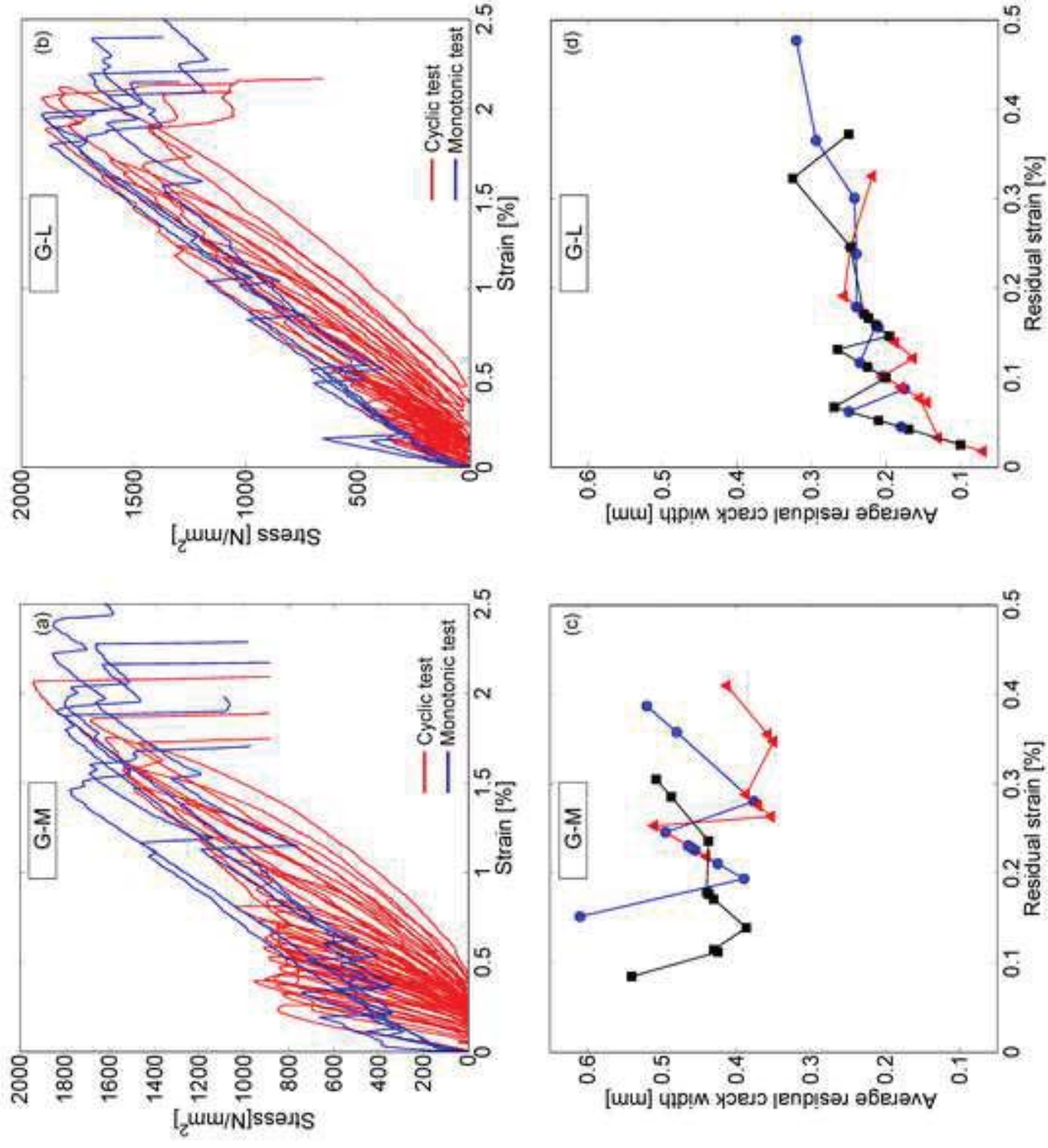


Figure 11
Click here to download high resolution image

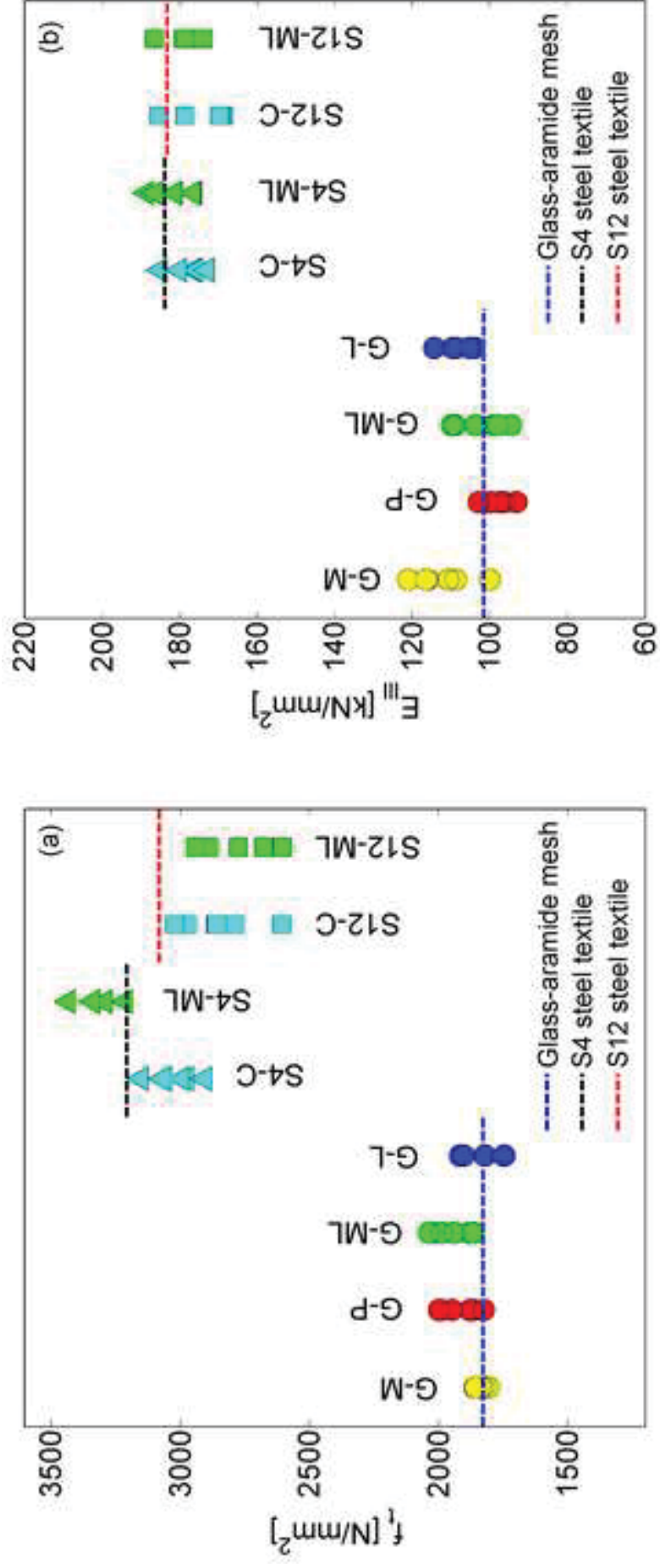


Figure 12
[Click here to download high resolution image](#)

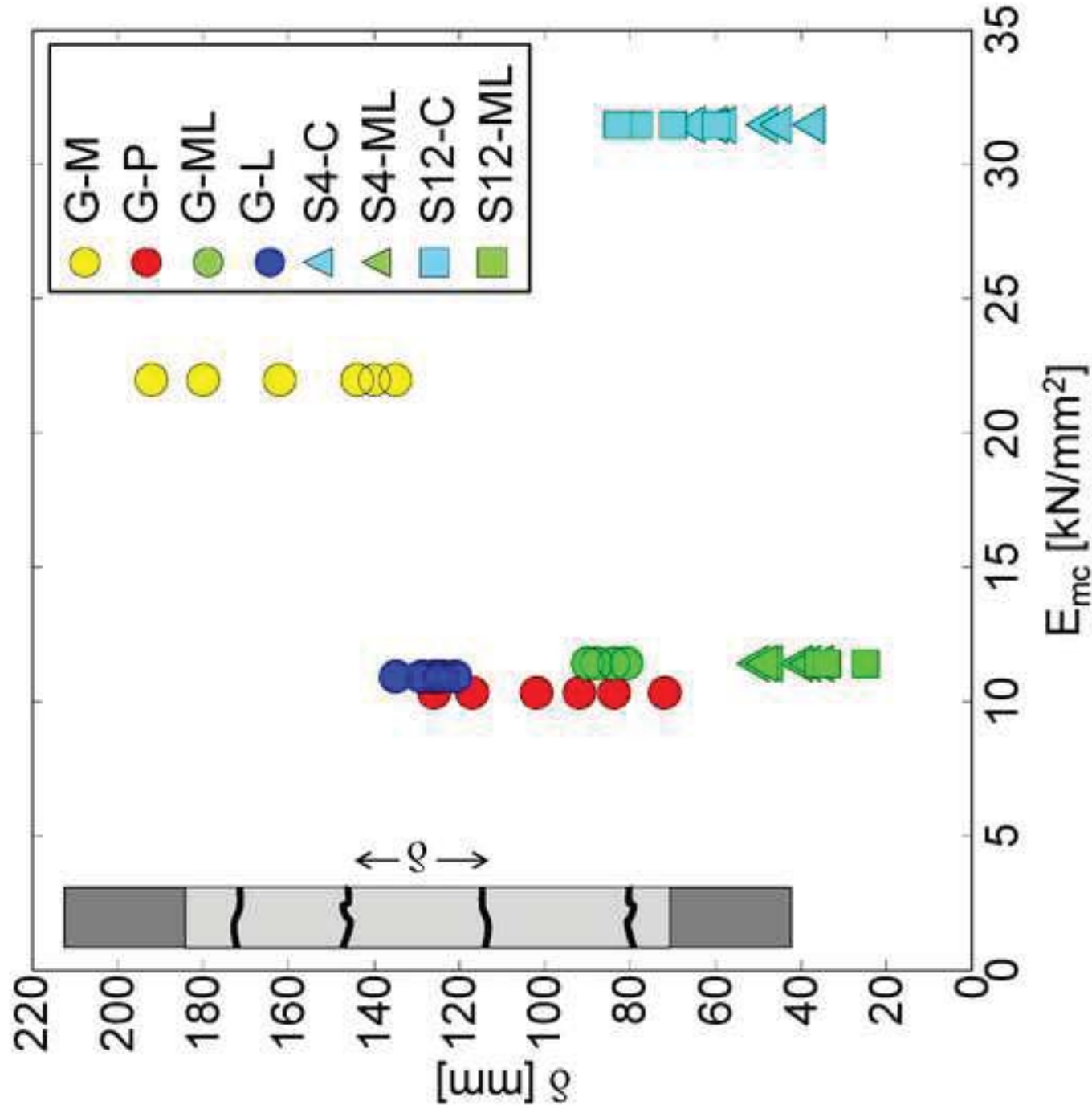


Figure 13
[Click here to download high resolution image](#)




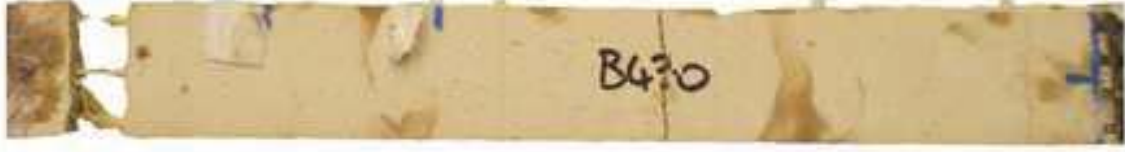




| | | | | | | | | |
|--|--|--|--|---|--|--|--|--------|
|  |  |  |  |  |  |  |  | |
| Series | G-M | G-P | G-ML | G-L | S4-C | S4-ML | S12-C | S12-ML |
| E_{mc} [kN/mm ²] | 22.0 | 10.3 | 11.4 | 10.9 | 31.5 | 11.4 | 31.5 | 11.4 |
| f_{mt} [N/mm ²] | 10.3 | 6.9 | 5.4 | 4.4 | 5.5 | 5.4 | 5.5 | 5.4 |
| $\langle \delta \rangle$ [mm] | 158 | 99 | 86 | 126 | 52 | 43 | 74 | 31 |

Figure 14
[Click here to download high resolution image](#)

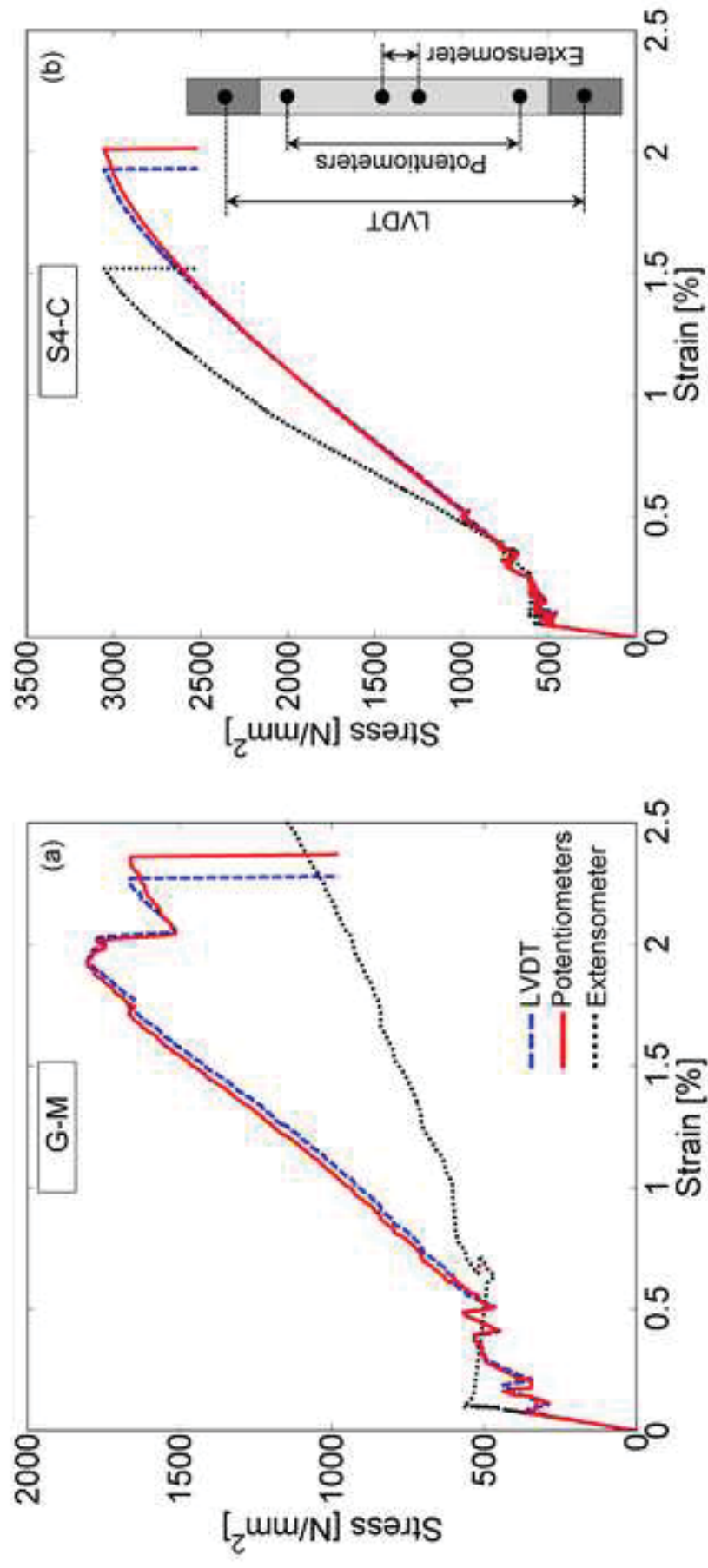


Figure 15
[Click here to download high resolution image](#)

